A multiscale Laplacian of Gaussian filtering approach to automated pulmonary nodule detection from whole-lung low-dose CT scans

Sergei V. Fotin[a], Anthony P. Reeves[a], Alberto M. Biancardi[a]
David F. Yankelevitz[b] and Claudia I. Henschke[b]

[a]School of Electrical and Computer Engineering, Cornell University,
Ithaca, NY 14853, USA;
[b]Department of Radiology, NewYork-Presbyterian Hospital - Weill Cornell Medical Center,
New York, NY 10021, USA

ABSTRACT

The primary stage of a pulmonary nodule detection system is typically a candidate generator that efficiently provides the centroid location and size estimate of candidate nodules. A scale-normalized Laplacian of Gaussian (LOG) filtering method presented in this paper has been found to provide high sensitivity along with precise locality and size estimation. This approach involves a computationally efficient algorithm that is designed to identify all solid nodules in a whole lung anisotropic CT scan.

This nodule candidate generator has been evaluated in conjunction with a set of discriminative features that target both isolated and attached nodules. The entire detection system was evaluated with respect to a size-enriched dataset of 656 whole-lung low-dose CT scans containing 459 solid nodules with diameter greater than 4 mm. Using a soft margin SVM classifier, and setting false positive rate of 10 per scan, we obtained a sensitivity of 97% for isolated, 93% for attached, and 89% for both nodule types combined. Furthermore, the LOG filter was shown to have good agreement with the radiologist ground truth for size estimation.

Keywords: Automated pulmonary nodule detection, Laplacian of Gaussian (LOG), algorithm evaluation and validation, computer-assisted diagnosis (CAD), computed tomography (CT).

1. INTRODUCTION

Laplacian of Gaussian (LOG) filtering has been used in many computer vision and image analysis applications for the task of multi-scale edge and ridge detection. The LOG filter has also been shown to be particularly good for enhancing blob-like objects that have an intensity different from that of background.[1] In the domain of computer-aided detection, LOG filters have been used for chest radiographs,[2] however their successful application for CT was limited,[3] mostly because of their computational complexity.

A symmetric LOG convolution kernel applied to an image will result in a high response when located over the center of a high intensity "blob" object, such as a nodule surrounded by low intensity parenchyma, when the size of the blob matches the central region of the LOG kernel . This approach also works for "attached" nodules that are close to or merged with an adjacent solid structure. The effect of fixed-scale filtering is illustrated in the two-dimensional example shown in Figure 1. For each synthetic nodule, we can see a corresponding maximum on the filtered image for the different degrees of its connectivity to the solid body.

With proper size normalization, LOG filtering also becomes an effective tool for estimating size without explicit nodule segmentation.[4,5] The characteristic scale of the kernel is directly related to the diameter of nodule to be detected: when the spherical zero-crossings surface of the kernel with scale σ^2 coincides with the surface of the perfect round nodule of diameter d, the following condition is satisfied: $d^2 = 12\sigma^2$ (or $d^2 = 4\sigma^2$ in one-dimensional case). Here, the corresponding size-normalized kernel has the maximum possible response across all the scales. Responses of the filters of different sizes to an image of fixed diameter nodule for a one-dimensional case are illustrated in Figure 2.

Send correspondence to Sergei V. Fotin, e-mail: svf3@cornell.edu, phone: 1 607 255 0963

Medical Imaging 2009: Computer-Aided Diagnosis, edited by Nico Karssemeijer, Maryellen L. Giger
Proc. of SPIE Vol. 7260, 72601Q · © 2009 SPIE · CCC code: 1605-7422/09/$18 · doi: 10.1117/12.811420

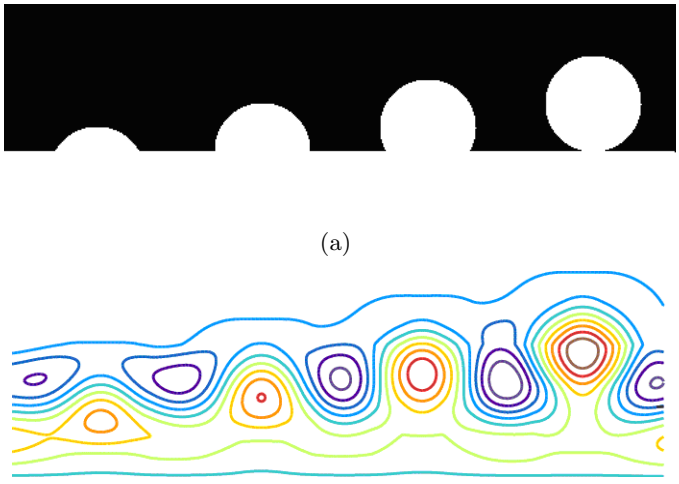

(a)

(b)

Figure 1. Illustration of LOG filtering with respect to location estimate: original two-dimensional synthetic model of attached nodules (a), contour plots of filter response with the kernel selected to match the nodule size (b).

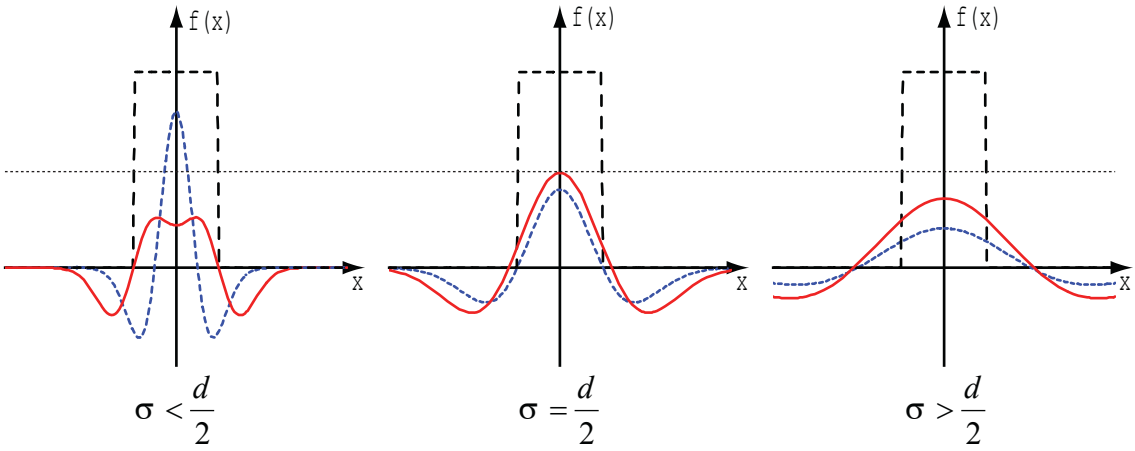

Figure 2. Illustration of LOG filtering with respect to size estimate: one-dimensional scale-normalized negated LOG kernels of different characteristic scales (curvy dashed line) are convolved with the model of the nodule represented by the box function (dashed box) of width d. Maximum response (solid line) is observed when the characteristic scale corresponds to the size of the nodule (i.e. LOG zero-crossings coincide with its boundary).

Table 1. Quantization of candidates sizes.

d_0	Working candidate diameters: $d_1 ... d_{10}$, mm										d_{11}
2.37	3.00	3.80	4.81	6.08	7.70	9.74	12.33	15.60	19.75	25.00	31.64

2. METHOD

The LOG filter properties for estimating nodule position and size are important for nodule candidate detection. Nodule candidates are identified by maxima in the four-dimensional multiscale image feature space created by filtering the 3D image with kernels of different size. The local maximum identifies the spatial location and the best matching size for a candidate nodule in that region of space.

In order to apply a scale-normalized LOG kernel $\sigma^2\nabla^2 G(x, y, z, \sigma^2)$ with characteristic scale σ^2 to the image $I(x, y, z)$, one needs to obtain the set of filtered images by computing multiple convolutions separately for each of the kernel sizes:

$$L(x, y, z, \sigma^2) = I(x, y, z) * \sigma^2\nabla^2 G(x, y, z, \sigma^2), \tag{1}$$

where $G(x, y, z, \sigma^2)$ is three-dimensional Gaussian with variance σ^2.

One efficient implementation of the multiscale LOG transform is to do the computation in the frequency domain with Gaussian kernels. Scale-normalized LOG kernel is the limit case of the difference of two Gaussians with different variances:

$$\sigma^2\nabla^2 G(x, y, z, \sigma^2) = \lim_{k\to 1} \frac{1}{1-k} \left(G(x, y, z, \sigma^2) - G(x, y, z, (k\sigma)^2) \right), \tag{2}$$

thus, after setting k to be nearly 1, we can rewrite the convolution as:

$$L(x, y, z, \sigma^2) \propto F^{-1} \left\{ F\left\{ I(x, y, z) \right\} \cdot F\left\{ G(x, y, z, \sigma^2) - G(x, y, z, (k\sigma)^2) \right\} \right\}. \tag{3}$$

With known transforms of the Gaussian function and by substituting the LOG characteristic scale by the candidate diameter, we obtain the following definition of nodule candidates search space:

$$C(x, y, z, d) \propto F^{-1} \left\{ F\left\{ I(x, y, z) \right\} \cdot \left(G\left(\nu, \omega, \xi, \frac{3}{\pi^2 d^2} \right) - G\left(\nu, \omega, \xi, \frac{3}{\pi^2 (kd)^2} \right) \right) \right\}. \tag{4}$$

Subsequently, the set of candidates is defined as local maxima in the candidates search space with respect to both location and diameter:

$$< x, y, z, d >_i = \text{argmaxlocal} \left\{ C(x, y, z, d) \right\}, \tag{5}$$

provided that candidates belong to subspace bounded by spatial lung extent and the working size range for the nodule candidates.

The most computationally intensive steps are the Fourier transforms: one needs to make one forward FFT on the original CT scan and one inverse transform for each processed kernel size. Extension of the algorithm to anisotropic image space is straightforward since directly scaled kernels can be used.

3. EXPERIMENT

In our experiments we used ten candidate sizes $d_1 \dots d_{10}$ exponentially increasing from 3 to 25 mm. In order to find maxima for boundary scales, two supplementary kernels for d_0 and d_{11} were added as shown in Table 1.

In addition to evaluation of the candidate generator with respect to sensitivity, we attempted to validate the quality of its size estimator. It was done using Bland-Altman analysis[6] by comparing size of the produced candidate to the size of the corresponding nodule as documented in the ground truth. The generator's positional accuracy was also evaluated by computing ellipsoids of inertia (EOI) centered at candidate location. With the assumption that better candidate location would result in better geometrical compactness of the candidate

Table 2. Image and scanner parameters

Axial image size	512 x 512
Slice thickness	1.25 mm
In-plane resolution	0.5 ... 0.8 mm
CT Scanner models	GE LightSpeed VCT/Pro16/Ultra
Beam	120 kVp, variable tube current
Convolution kernel	BONE

Table 3. Amount of documented nodules in the original and enriched datasets.

Nodule diameter range	Original	Enriched
< 4 mm	401	599
≥ 4 mm	81	459
≥ 10 mm	9	63

(ratio of the longest to the shortest axis of EOI), we compared the LOG-based candidate generator to the volume occupancy curve (VOC) based generator reported in Enquobahrie et al.[7] A spherical nodule with the candidate placed exactly at its center would result in the compactness value of 1.

We also applied the set of the features, previously developed by our research group[7] to assess the effectiveness of the entire detection system based on LOG-filtering. The following features were used: LOG filter response, contrast ratio of positive part to negative part of the volumes of support, ellipsoid of inertia compactness computed from geometrical moments, primary and secondary attachment, and distances to the lung boundary and to the airway tree.

Performance evaluation was done with respect to a size-enriched dataset of 656 whole-lung low-dose CT scans from Weill Cornell Medical Center database containing 459 solid nodules (276 isolated and 183 attached) with diameter greater than 4 mm. Image and scanner parameters are shown in Table 2. Our original (non-enriched) dataset[7] consisted of only 250 sequential asymptomatic cases, where tiny lesions smaller than 4 mm were dominant. To enhance the dataset, we intentionally included new 406 cases containing at least one solid nodule of diameter 4 mm or larger. We selected the size of 4 mm as the lower bound criteria for enrichment because this size range is the prime detection target and is less affected by size estimation error due to limited visibility as delineated in Fotin et al.[8] Nodule visibility, in its turn, depends on the scanner and image acquisition parameters; e.g. higher axial resolution would facilitate the detection of smaller nodules.

After the database was enriched, the fraction of nodules greater than 10 mm increased from 2% to 6% and the fraction of nodules greater than 4 mm increased from 17% to 43%. Amount of nodules in each category is shown in Table 3, while the distributions of nodule sizes in the original (sequential) and enriched datasets are shown in Figure 3. This change in evaluation subset allowed us to extend and test the capabilities of our detection system on the nodules that are more clinically important while providing better accuracy of performance evaluation.

For quantitative performance assessment, the evaluation set was split in half case-wise for training and testing. The flowchart of the experiment setup based on the LOG candidate generator is shown in Figure 4. The algorithm was optimized with the help of soft margin SVM classifier with linear kernel[9] three times: for detection of isolated, attached and all types of nodules independently using the development (train) subset. Obtained system configurations were applied to the test set and free-response receiver operating characteristics (FROC) were constructed.

4. RESULTS

The LOG-based generator was able to produce stable local maxima in candidate search space for all 459 nodules in the evaluation subset. With the described size quantization, the number of maxima defined for the entire chest scan was about 100,000. After limiting maxima locations to the lung region and thresholding the filter

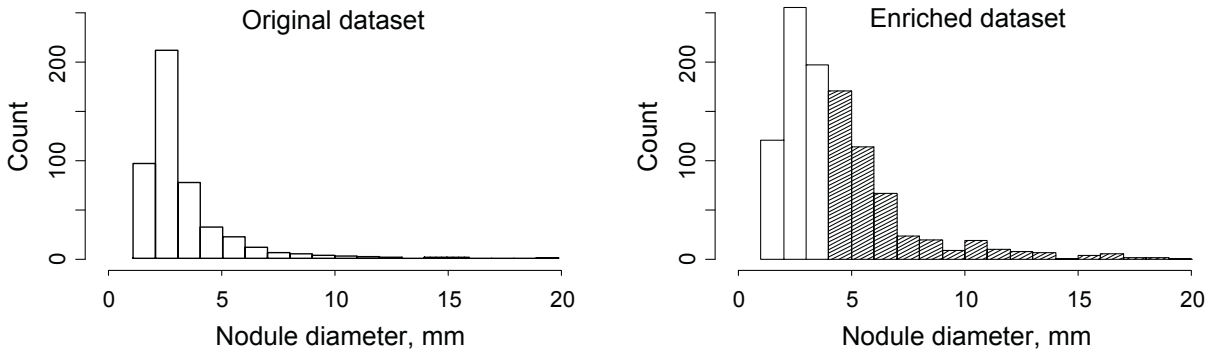

(a) (b)

Figure 3. Distribution of nodules in the original (a) and enriched (b) datasets; shaded bins represent the evaluation subset.

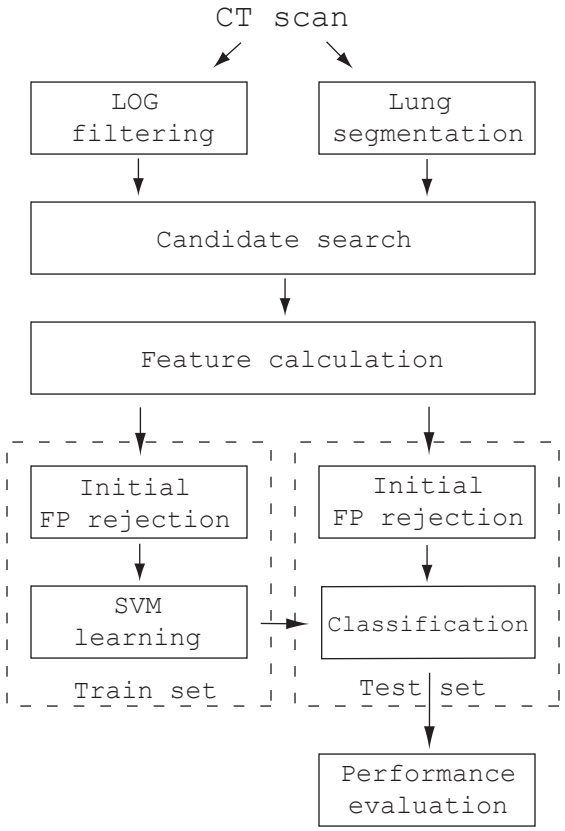

Figure 4. The flowchart for the evaluation of the experimental detection system.

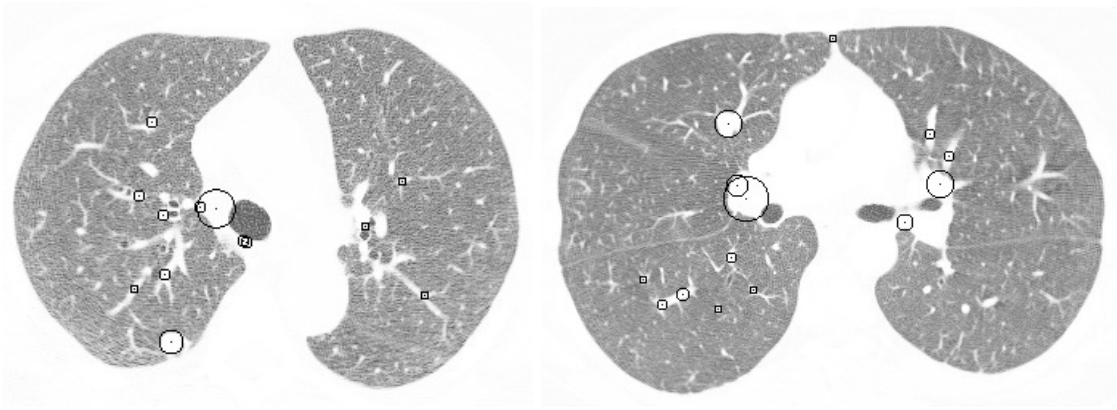

(a) (b)

Figure 5. An output of the LOG-based generator shows potential nodule candidate locations after suppression of low-response candidates on a slice of 3D image: case CU1920 (a), CU2829 (b). Circles are centered at candidate locations, while the diameter shows the scale with maximum filter response.

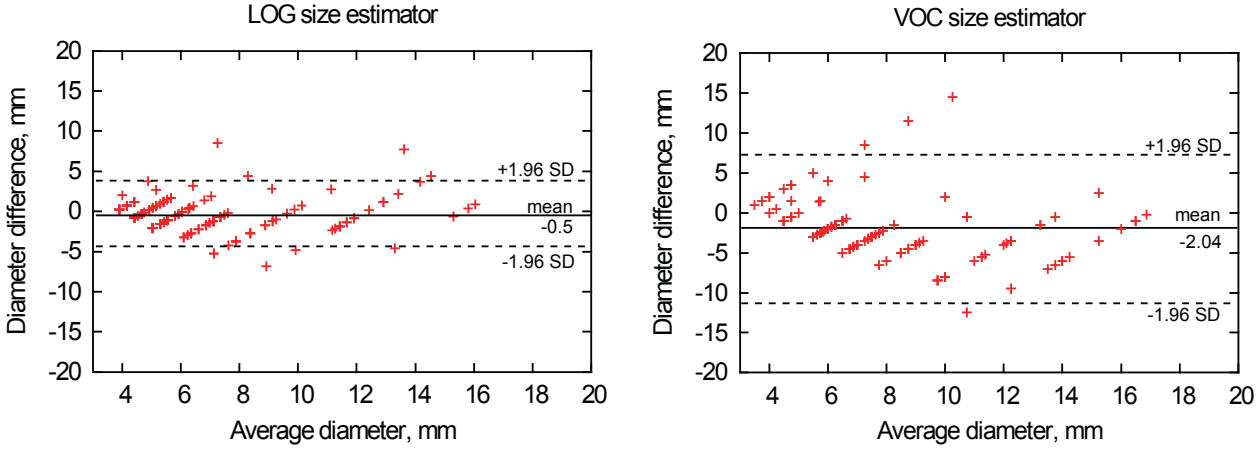

(a) (b)

Figure 6. Bland - Altman analysis of two sizing methods: LOG (a) and VOC (b) for attached nodules. Diagonal patterns in data points are caused by discretization of both manual and automated nodule size estimates.

response, the number of candidates was reduced to the order of 1000 candidates per case. An example outputs of the candidate generator are shown in Figure 5. Most of the candidates were vessel bifurcations and mediastinal abnormalities that were further reduced by geometrical attachment filters.

The difference between two LOG and VOC based generators with respect to the accuracy of size measurement against the size defined by the radiologists is shown in Figure 6. The 95% confidence intervals of the difference between automated and manual size measurements were -0.50 ± 4.52 and -2.06 ± 9.16 for LOG and VOC generator respectively. Note, that the diagonal point patterns on the plot were caused by quantization of nodule size estimates.

Geometrical position accuracy as measured by the compactness of the nodule is depicted in Figure 7. 90% of all nodules had the value less than 1.27 for LOG and 1.77 for VOC-based generator.

Figure 8 shows the FROC curves on the test subset obtained by the detection system for isolated, attached and all solid nodules.

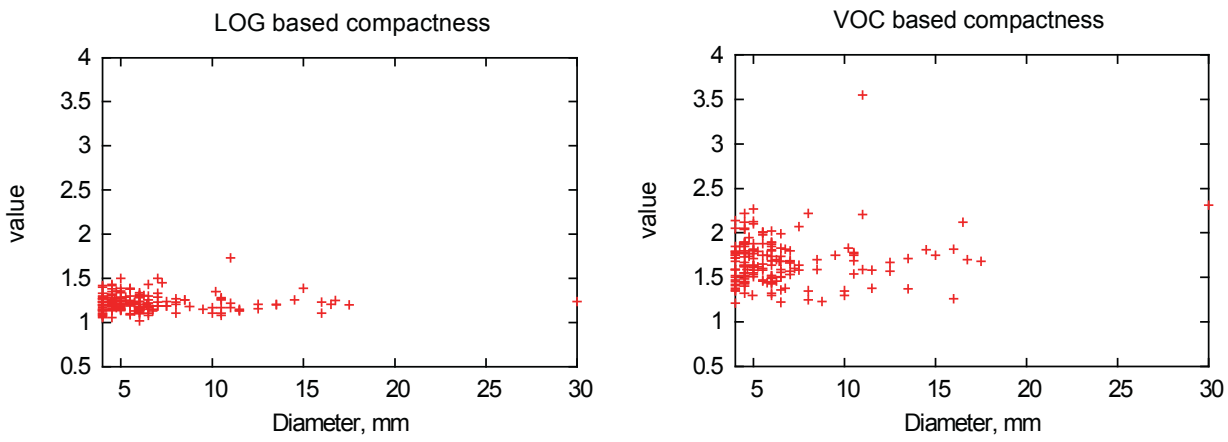

(a) (b)

Figure 7. Comparison of "Ellipsoid of inertia compactness" feature for attached nodules using LOG (a) and VOC (b) estimators. Diameter of the nodule is taken from the ground truth.

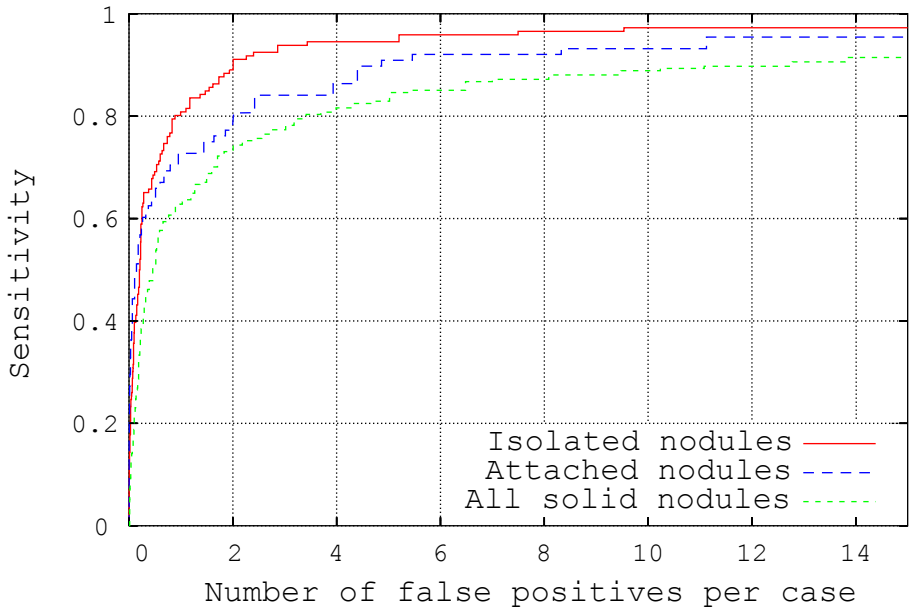

Figure 8. Performance of the detection system on solid nodules greater than 4 mm.

5. DISCUSSION

We can see that LOG-based filtering can be used as efficient candidate generator. In addition to high sensitivity, the candidate generator provides nodule size measurements that are very close to ground truth values and have a very little bias. Also, the generator results in lesser spread of the compactness feature which is a sign of better positional accuracy. Consequently, all subsequent features that rely on accurate size and location measurements had higher discriminative power as illustrated by the FROC curves.

6. CONCLUSION

A fast and efficient technique for the automated detection of solid pulmonary nodules from lung CT scans is presented and evaluated.

A pulmonary nodule detection system based on scale-normalized LOG filtering and accompanied with moment, attachment and proximity features can achieve high detection performance on whole-lung low-dose CT scans. Moreover, we showed that LOG candidate generator had higher sensitivity, position and size estimation accuracy on attached nodules than previously employed VOC generator. Finally, enrichment of a dataset with large nodules is important for gaining in performance in the desired nodule size range.

7. ACKNOWLEDGMENTS

This research was supported in part by NIH grant R33CA101110 and the Flight Attendants' Medical Research Institute. Drs. Henschke, Yankelevitz and Reeves are co-inventors on a patent and other pending patents which are owned by Cornell Research Foundation (CRF) who non-exclusively licenses them to General Electric for technology involving detection and characterization of nodules in many medical situations, including measurement of nodules. They receive royalties from CRF pursuant to Cornell policy, which in turn is consistent with the Bayh-Dole Act. They are also inventors on a pending patent application for lesion measurement. Dr. Yankelevitz is an inventor on a pending patent owned by PneumRx related to biopsy needles, serves as a medical advisor to them, and holds an equity interest in PneumRx.

REFERENCES

[1] Lindeberg, T., "Detecting salient blob-like image structures and their scales with a scale-space primal sketch: A method for focus-of-attention," *International Journal of Computer Vision* **11**(4), 283–318 (1993).

[2] Schilham, A., van Ginneken, B., and Loog, M., "Multi-scale Nodule Detection in Chest Radiographs," *LECTURE NOTES IN COMPUTER SCIENCE* , 602–609 (2003).

[3] Dolejsı, M. and Kybic, J., "Automatic Two-Step Detection of Pulmonary Nodules," in [*Proceedings of SPIE*], **6514**, 65143J (2007).

[4] Reeves, A., Chan, A., Yankelevitz, D., Henschke, C., Kressler, B., and Kostis, W., "On measuring the change in size of pulmonary nodules," *Medical Imaging, IEEE Transactions on* **25**(4), 435–450 (2006).

[5] Diciotti, S., Lombardo, S., Coppini, G., Grassi, L., Petrolo, L., Picozzi, G., Falchini, M., and Mascalchi, M., "The characteristic scale as a consistent indicator of lung nodule size in CT imaging," in [*CARS*], S182–183 (2008).

[6] Bland, J. and Altman, D., "Measuring agreement in method comparison studies," *Statistical Methods in Medical Research* **8**(2), 135 (1999).

[7] Enquobahrie, A., Reeves, A., Yankelevitz, D., and Henschke, C., "Automated Detection of Small Solid Pulmonary Nodules in Whole Lung CT Scans from a Lung Cancer Screening Study," *Academic Radiology* **14**(5), 579–593 (2007).

[8] Fotin, S., Reeves, A., Yankelevitz, D., and Henschke, C., "The impact of pulmonary nodule size estimation accuracy on the measured performance of automated nodule detection systems," in [*Proceedings of SPIE*], **6915**, 69151G (2008).

[9] Joachims, T., "Making large-Scale SVM Learning Practical. Advances in Kernel Methods-Support Vector Learning, B. Schölkopf and C. Burges and A. Smola," (1999).